Pergamon

Adv. Space Res. Vol. 15, No. 8/9, pp. (8/9)85–(8/9)92, 1995
1995 COSPAR
Printed in Great Britain
0273–1177/95 $9.50 + 0.00

0273-1177(94)00088-3

PROPAGATION AND DAMPING OF BROADBAND UPSTREAM WHISTLERS

D. S. Orlowski,* C. T. Russell,* D. Krauss-Varban,**
N. Omidi** and M. F. Thomsen***

* *Institute of Geophysics and Planetary Physics, University of California, Los Angeles, CA 90024, U.S.A.*
** *Department of Electrical and Computer Engineering and California Space Institute, University of California at San Diego, La Jolla, CA, U.S.A.*
*** *Los Alamos National Laboratory, Los Alamos, NM, U.S.A.*

ABSTRACT

Previous studies indicated that damping rates of upstream whistlers strongly depend on the details of the electron distribution function. Moreover, detailed analysis of Doppler-shift and whistler dispersion relation indicated that upstream whistlers propagate obliquely in a broad band. In this paper we present results of a kinetic calculation of damping lengths of wide-band whistlers using the sum of 7-drifting bi-Maxwellian electron distributions as a best fit to the ISEE 1 electron data. For 2 cases, when upstream whistlers are observed, convective damping lengths derived from ISEE magnetic field and ephemeris data are compared with theoretical results. We find that the calculated convective damping lengths are consistent with the data and that upstream whistlers remain marginally stable. We also show that the slope of plasma frame spectra of upstream whistlers, obtained by direct fitting of the observed spectra is between 5 and 7 with a sharp lower frequency cutoff corresponding to a wavelength of about one ion inertial length. When the solar wind velocity is directed largely along the wave normal of the upstream whistlers the polarization of the right hand waves becomes reversed and low frequencies are switched to high resulting in a peaked spectrum with a strong high frequency cutoff. The overall spectral, wave and particle characteristics, proximity to the shock as well as propagation and damping properties indicate that these waves cannot be generated locally. Instead the observed upstream whistlers arise in the shock ramp most likely by a variety of cross-field drift and/or anisotropy driven instabilities.

INTRODUCTION

A frequent phenomenon upstream of planetary bow shocks is a propagating whistler mode wave that at the Earth is observed in the spacecraft frame close to one Hertz. This paper aims to address in detail the question of the variablility, formation of the spectral shapes and observed polarizations of these upstream whistlers as well as to address the thus far controversial question of the generation and damping of whistlers in the upstream region. We derive a fitting procedure and calculate plasma frame power spectral densities for 2 cases. We present the results of the detailed modeling of the upstream electron distribution functions in the Earth's foreshock using a 7 drifting bi-Maxwellian fit as well as the results of calculations of linear damping rates using Vlasov theory for the same 2 cases in order to examine how the fine structure of the suprathermal electron distribution influences dispersive properties of upstream whistlers. Further we discuss and compare convective damping lengths calculated from theory with the attenuation lengths derived from ISEE magnetic field data. We also discuss the results of the fitting procedure and compare the resulting spectral shapes to those observed within the shock. Finally we discuss and interpret the theoretical and experimental work relevant to the generation of upstream whistlersin view of the results of this paper on damping. The theoretical calculations are carriedout using a newly developed kinetic solver /1/.

FITTING AN ANALYTICAL MODEL

We assume that the spectral density of the upstream whistlers in the plasma frame can be well approximated by a power law of the form $S_{xx} = a/\omega^q$; $q > 1$where a,q and $\Delta\omega$ are the fitting parameters. The wave power at frequency w within the frequency band $\delta\omega << \Delta\omega$ has the form.

$$P_{xx}(\omega, \delta\omega) = \int_{\omega - \delta\omega/2}^{\omega + \delta\omega/2} S_{xx}(\nu)\, d\nu = \frac{\omega}{2^{1-q}(q-1)}\left[\left(2 + \frac{\delta\omega}{\omega}\right)^{1-q} - \left(2 - \frac{\delta\omega}{\omega}\right)^{1-q}\right] \quad (1)$$

In the spacecraft frame the corresponding power will be:

$$P_{xx}(\omega', \delta\omega') = \int_{\omega' - \delta\omega\,1/2}^{\omega' + \delta\omega\,1/2} S'_{xx}(\nu')\, d\nu' = S'_{xx}(\omega') \cdot \delta\omega' \quad (2)$$

where: $<S_{xx}(\omega')>$ is an estimate of the spectral density in the spacecraft frame; $\Delta\omega'$ is a Doppler-shifted bandwidth. Also the Doppler-Shift and dispersion relation have the form:

$$\omega' = \omega + \mathbf{k}.\mathbf{V}_p \quad (3)$$

$$D(\omega, \mathbf{k}) = 0 \quad (4)$$

Since wave power is invariant for a Doppler-shift transformation the solution of equations 1-4 allow us to evaluate the spectral shape in the spacecraft frame. However, this spectral shape $<(S_{xx}(\omega'))>$ is not what is in reality observed. This is due to the fact that commonly used spectral analysis techniques such as power spectra from the FFT asume a symmetric spectrum and do not discriminate between different polarizations of the wave. In fact, the spectral form is non-symmetric in the spacecraft frame and is polarization dependent. The observed power spectral density $<(S_{xx}(\omega''))>_{obs}, \omega'' \geq 0$ is expressed by:

$$<(S_{xx}(\omega''))>_{obs} = [\eta(\omega') <(S_{xx}(\omega'))>]_R + [\eta(-\omega') <S_{xx}(\omega')>]_L$$

The above formula describes the fact that the observed spectrum is created by overlapping two spectra with opposite polarizations indicated by R (right handed) and L (left handed). As a consequence, the observed spectrum cannot be exactly mapped back into the plasma frame.

THE RESULTS OF FITTING PLASMA FRAME SPECTRA

CASE 1. Plasma and wave parameters we used are the following: $V_{sw} = 355$ km/s; $\theta_{Bk} = 31$ deg; $\theta_{kV} = 63$ deg; $B_o = 8.4$ nT and $n_p = 9$ cm^{-3}, $T_p = 15.5$ eV. The lighter shaded spectrum shown in Figure 1 is the spacecraft frame spectrum that fits the observed spectrum (indicated by filled circles) starting at about 2 Hz at the evident break in the observed spectrum between the low frequency part of the spectrum with the relatively flat slope $q < 2$ per decade and the steep spectrum with $q = 7$.

CASE 2. Figure 2 shows the result of the fitting procedure for this case. Plasma and wave parameters were $V_{sw} = 330$ km/s; $\theta_{Bk} = 31$ deg; $\theta_{kV} = 17$ deg, $B_o = 4.3$ nT and $n_p = 5$ cm^{-3}, $T_p = 13.0$ eV. The lighter shaded spectrum indicates the spacecraft frame spectrum that fits to the observed spectrum (indicated by crosses). The sharp peak and cutoff of the observed spectrum is well represented. In contrast the plasma

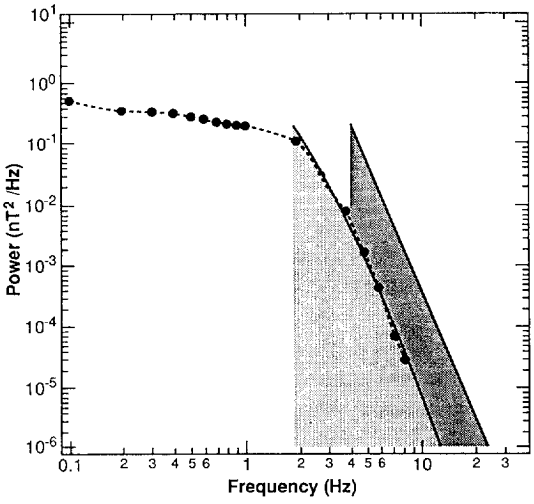

Figure 1. Plasma frame (fitted) spectrum (dark gray), calculated, observed spectrum (light gray) and measured spectrum of upstream whistlers within the time interval between 2315 and 2317 UT on July 22, 1978.

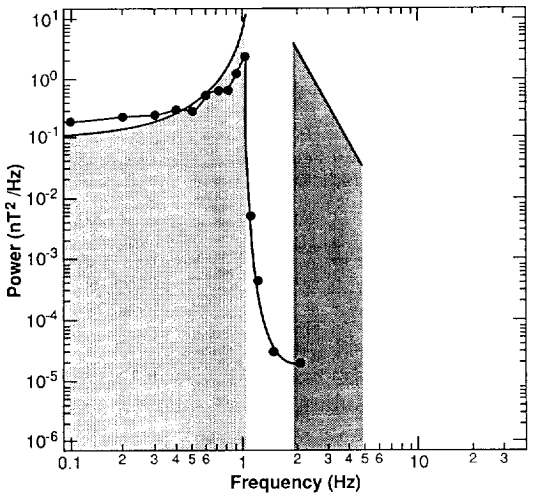

Figure 2. Plasma frame (fitted) spectrum (dark gray), calculated, observed spectrum (light gray) and measured spectrum of upstream whistlers within the time interval between 2022 and 2024 UT on December 15, 1977. The waves are predominantly L.H. in spacecraft frame.

frame spectrum (dark shade) is monotonic with a spectral density slope, q = 5.6.

DETERMINATION OF DAMPING PROPERTIES OF UPSTREAM WHISTLERS

In order to evaluate the attenuation length, ΔL_c we first determine the shock velocity as, $V_{sh} = \mathbf{S}.\mathbf{n}/\Delta t$ where: **S** is the spacecraft separation vector; **n** is a unit vector parallel to the shock normal, Δt - time lag between two spacecraft obtained from correlation analysis. After correcting for the spacecraft velocity in the plasma rest frame, the estimate of convective damping length is calculated from the following formula:

$$L_c = \mid L_{cf}^* - L_{ci}^* \mid ;$$

L_{ci}^* (L_{cf}^*) is a distance from the wave source to the spacecraft along magnetic field line at time t_i, (t_f) corrected for convection of solar wind, ΔL_c^* is a attenuation length corrected for convection of wave packet along the field aligned ray path from the source on the shock surface up to the observation site. The above approximation is valid under following assumptions: 1) shock speed along B_o and shock normal direction at the time of the observation is the same as during the shock crossing (some time earlier). 2) ray paths of upstream whistlers are field aligned. 3) the time of flight effect is small but finite e.g. $\mathbf{V}_{sh}.\mathbf{b}_o << \mathbf{V}_{g||}$, $\mathbf{V}_{sc}.\mathbf{b}_o << \mathbf{V}_{g||}$ and $\Delta L_{cf}/V_{g||} << \mid t_f - t_i \mid$. We find following ranges of attenuation length estimate: case 1, $\Delta L_c^* = 1160$ to 2070 km, case 2, $\Delta L_c^* = 150$ to 260 km. The geometry used in calculations of ΔL_c, L_{ci}^* and L_{cf}^* is shown in Figure 3. In order to calculate damping rates we use plasma and wave parameters assuming a Maxwellian proton distribution. Our aim is to specifically model the part of the distribution that is most likely to interact with the upstream whistlers. In order to achieve good correspondence between observed and modeled electron pitch angle scans we use a 7 drifting bi-temperature Maxwellian fit. Using the measured plasma properties and modeled electron distribution function we then solve the full electromagnetic dispersion relation.

CASE 1. Figure 4 shows our fit to the measured distribution presented for case 1. In both of these figures, the three lowest energy levels are shifted up (by ½, 1, and 1½ decades respectively) for better separation. The results of the linear Vlasov theory calculations making use of this fit and the plasma data are shown in Figure 5. In Figure 5 the upper panel shows the real part of the dispersion relation calculated in the spacecraft frame, the middle panel shows damping rates and the lower panel shows the convective damping length as a function of wave number. The damping length is given both normalized

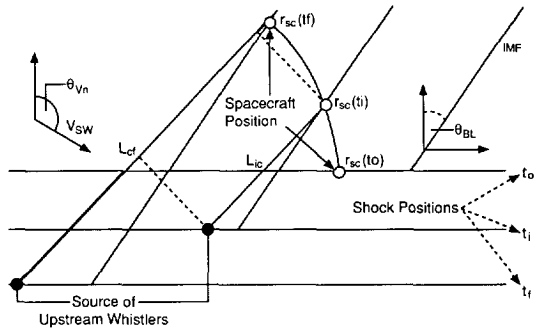

Figure 3. The geometry used for calculations of the power e-fold attenuation length from ISEE data. The hollow circles indicate spacecraft position r_{sc} at times t_o - shock crossing time, t_i - initial time, t_f - final time respectively which must satisfy following condition: $Ln[P(t_i)/P(t_f)]=1$; L_{ci} is the initial distance from the source of the waves (black filled circle) and L_{cf} is the final distance from the source of the waves where both are calculated taking into account the convection of solar wind. The bold part of L_{cf} is an e-folding attenuation distance $\Delta L_c = | L_{cf}^* - L_{ci}^* |$. θ_{Bn} is an angle between IMF and shock normal and θ_{vn} is an angle between solar wind velocity and the shock normal. Relevant shock positions are also indicated.

by the proton inertial length and in km. The dark shading indicates the band width of the waves as relevant to the observations. The solid lines correspond to the 7 drifting bi-Maxwellian fit, the dashed lines show results for a single Maxwellian. The dispersion relation in the upper panel clearly indicates that the spectrum is dominated by the original polarization of the waves ($\omega > 0$). It is also clear that in this case the fine structure of the electron distribution represented by the 7 drifting bi-Maxwellian fit does not affect the real part of the dispersion (solid and dashed lines nearly identical). However, the influence on the growth rate is significant as seen in the middle panel of Figure 5. The existence of the backstreaming beam seems to cause the damping rate to decrease from about 1.3 to 0.1 Ω_p within the upstream wave

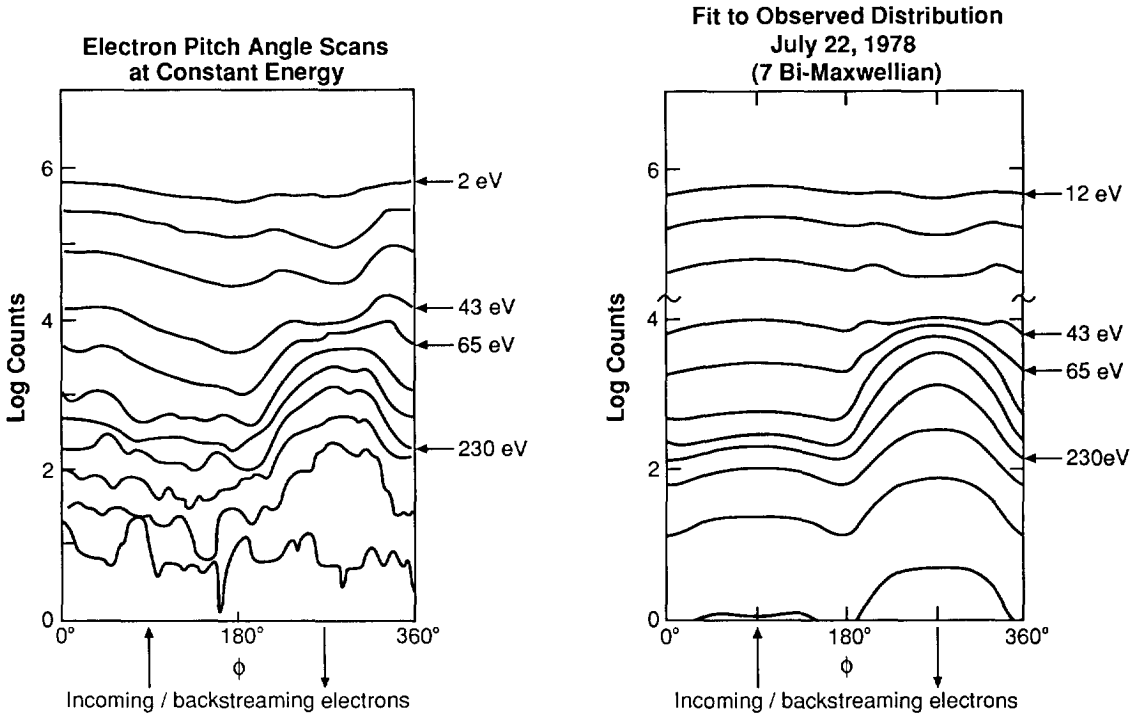

Figure 4. The observed electron flux pitch angle distribution observed (left) and modeled (right) for the time interval between 2315 and 2317 UT on July 22, 1978 (case 1). The modeled electron flux pitch angle distribution was obtained using 7 bitemperature Maxwellian fit. The relative direction of the electrons with respect to the magnetic field is also indicated.

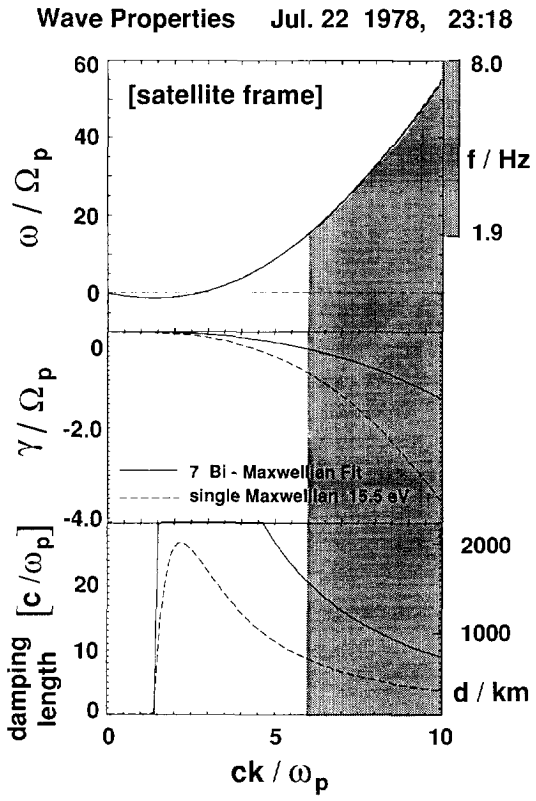

Figure 5. The results of the solution of the full electromagnetic dispersion relation for case 1 e.g. 2315 and 2317 UT on July 22, 1978. Real part of dispersion relation in spacecraft frame (upper panel), imaginary part of the dispersion relation - damping rate (middle panel) and convective damping length (lower panel). The shaded areas indicate the bandwidth of upstream whistlers.

bandwidth (solid line) more than 50% smaller than the damping rate calculated from a single Maxwellian approximation of the electron distribution (dashed line). We note that within the full range of frequencies the upstream whistler waves were found to be stable with significant damping rates. The lower panel of Figure 5 shows the results of the calculation of the convective damping lengths $\Lambda_c = V_g^*/\gamma$. For simplicity, we have calculated here the convected group velocity along the wave vector, $V_g^* = \omega/k - \mathbf{V}_{sw}.\mathbf{k}$. Since $\theta_{Bk} \cong 31$ deg for both cases, V_g^* should cause a slight consistent underestimation of convective damping length along the magnetic field line. It is clearly seen that Λ_c is very sensitive to the fine structure of the electron distribution. The lower panel of Figure 6 (right) shows that the single Maxwellian fit predicts Λ_c to be in the range of 450 to 600 km, inconsistent with experimental estimates, while the use of the 7 drifting bi-Maxwellian fit enables us to correctly predict the Λ_c ranging from 800 to 1600 km. The ability of linear Vlasov theory to correctly predict Λ_c for these small amplitude whistlers strengthens our conclusion about the stability of the waves based on linear theory versus growth.

CASE 2: The measured electron distributions in the form of pitch angle flux contours and our fit for case 2 is shown in Figure 6. The dashed lines in Figure 6 indicate that no attempt has been made to match these to the observed levels, which for 2 lowest energies can be shown to originate from photoelectrons. Using the measured plasma properties and the modeled electron distribution function we again solve the full electromagnetic dispersion relation. The results are shown in Figure 7. The dark shading indicates the bandwidth of upstream whistlers as relevant to the wave data for case 2. The dispersion relation (upper panel) clearly indicates that the spectrum is dominated by left handed waves. Note the threshold for finite (positive) group velocity matches well with the observed cut-off of the waves at ~1 Hz. It is also clear that the fine structure of the electron distribution affects the real part of the dispersion only slightly in this case. Also, the effect on the growth rate seem not to be as significant as in case 1. The overall damping rate, however, ranges from about -5 to -1 Ω_p within the wave band. We note that also for this case within the full range of frequencies the upstream whistlers were found to be significantly

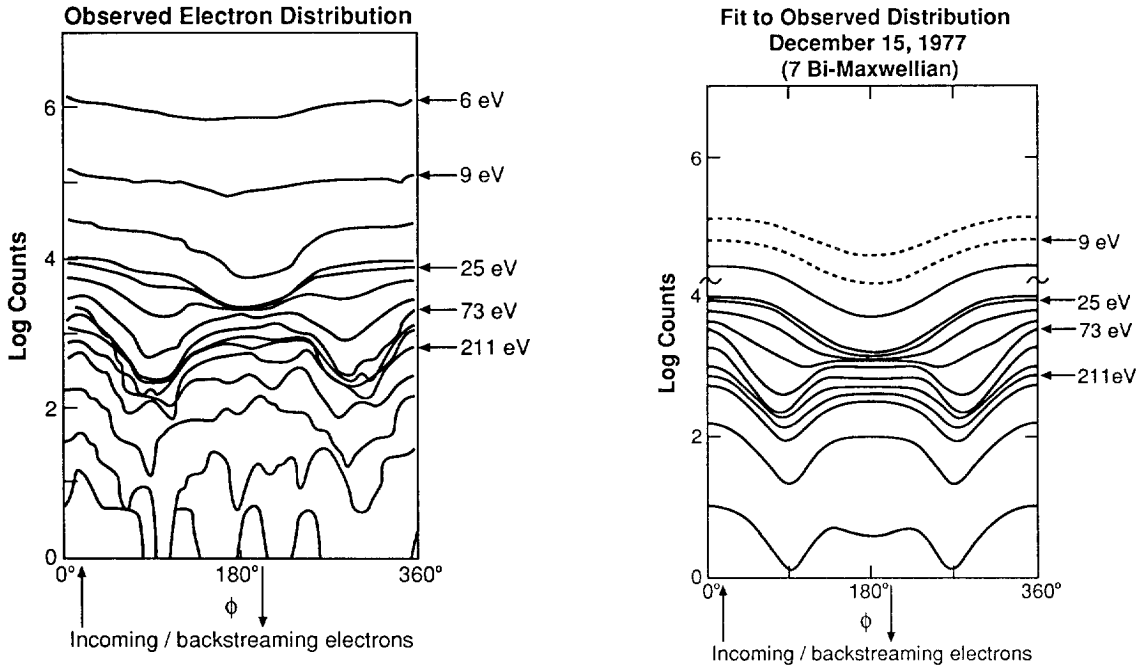

Figure 6. The electron flux pitch angle distribution observed (left) and modeled, fitted (right) for the time interval between 2022 and 2024 UT on December 15, 1977 (case 2).

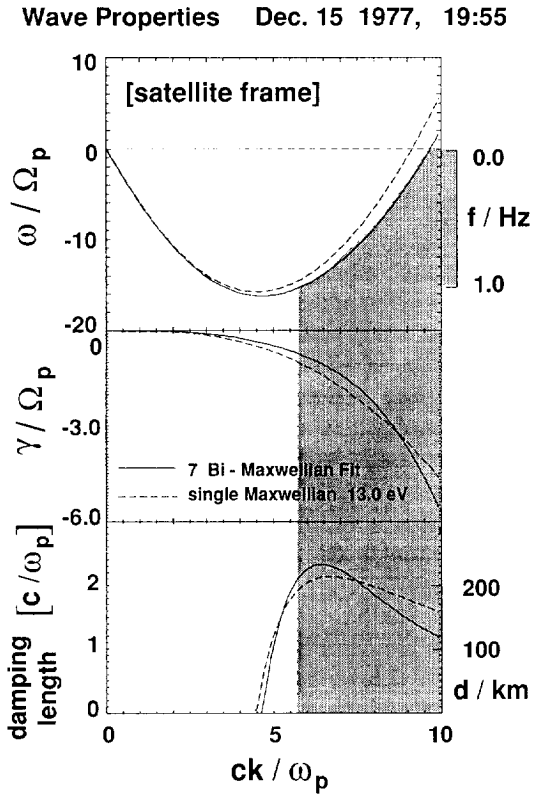

Figure 7. The results of the solution of the full electromagnetic dispersion relation for case 2 e.g. 2022 and 2024 UT on December 15, 1977. Real part of the dispersion relation in the spacecraft frame (upper panel); imaginary part of the dispersion relation - damping rate (middle panel) and convective damping length (lower panel). The shaded area indicates bandwidth of upstream whistlers.

damped. The lower panel of Figure 7 shows the results of the calculation of Λ_c. As it is clearly seen from this figure, the single as well as 7 drifting bi-Maxwellian fit predicts Λ_c within the range of 120 to 220 km, consistent with derived experimental estimates. Also note that the observed band is indeed that part of the spectrum for which the predicted damping lengths are large.

DISCUSSION

Spectral modeling. The upstream whistlers observed as RH or LH in the spacecraft frame have a common wide band spectral shape in the plasma frame well approximated by a power law, which shape indicates that they originate from a wide band source. The slopes of modeled plasma frame spectra are 7 and 5.6 respectively for case 1 and 2. Those slopes are steeper than the average slope of 4 ± 0.5 obtained in /2/ from a statistical study. There may be several reasons for this apparent discrepancy. First, observations were made at different locations. Second, have most of their spectral points are above 10 Hz outside of our fitting range. Since the whistlers with higher frequencies damp faster traveling along the ray path therefore, the spectrum obtained upstream may be steeper than that at the shock. However, for $q=4$ the power of the waves within the frequency 10-100 Hz, will be about 1000 times smaller than within the adjacent range 1-10 Hz that we consider. We note that for both intervals considered the lower frequency cutoff was $ck/\omega_{pi}\cong 2\pi$ corresponding to a largest wavelength of c/ω_{pi} which is close to the average thickness of the shock.

Whistler damping. We find that, for the upstream whistlers with the observed properties, the fine structure of the electron distribution function around the backstreaming electron beam typically observed in the foreshock may act to increase (case 2) or decrease (case 1) the damping of the waves. These small changes may affect the convective damping length up to about one order of magnitude, allowing whistlers at times to reach great distances as observed by /3,4,5,6,7/. In both cases we find upstream whistlers to be stable or marginally stable within their broad frequency band. Since the fine structure of the electron distribution function is highly variable with position with respect to the morphological boundaries of the foreshock /8/ the question of whether or not, in a specific case, the shock generated whistlers are able to reach far upstream or will be damped near the shock, depends on the details of their complicated ray paths and the electron distribution they encounter. In the plasma frame a broad band spectrum is found with a steep power law spectrum with a spectral index of about 5 and a lower frequency cutoff corresponding to a wavelength of close to the ion inertial length. When Doppler-shifting of this spectrum is weak the wave remain right handed in the spacecraft frame but when Doppler shifting is strong these waves undergo a reversal of polarization and the high frequencies are shifted to low and vice versa. Then the sharp lower frequency cutoff becomes a high frequency cutoff and the spectrum terminates in a peak rather than "power law" decrease.

CONCLUSIONS

In this report we have shown, using 2 detailed case studies, that upstream whistlers constitute wide band emissions with properties consistent with the shock generation. Moreover, while fine features of the electron distribution function in the foreshock, invoked by /9/ may influence whistler dispersive properties, they do not result in instability but rather in moderating the Landau damping of the whistler waves with the observed properties.

ACKNOWLEDGMENTS

This work was supported by National Aeronautics and Space Administration under research grant NAGW-2886 at UCLA, grant NAG5-1492 of the Space Physics Theory Program at UCSD and grant from D.O.D supported by NASA SR&T #18,061 at LANL. Computational facilities were provided by NSF San Diego Supercomputer Center.

REFERENCES

1. D. Krauss-Varban, N. Omidi, and K.B. Quest, Mode properties of low frequency waves: kinetic theory versus Hall-MHD, *J. Geophys. Res.*, *99*, 5987-6009, 1994.

2. P. Rodriguez, and D.A. Gurnett,Electrostatic and elelctomagnetic turbulence associated with Earth's bow shock, *J.Geophys.Res., 80*, 19-27,1975.

3. D.H. Fairfield, Whistler waves observed upstream of collisionless shocks, *J. Geophys. Res., 79*, 1368-1378, 1974.

4. M.M. Hoppe and C.T. Russell, L.A. Frank, T.E. Eastman and E.W. Greenstadt, Upstream hydromagnetic waves and their association with backstreaming ion population: ISEE 1 and 2 observations, *J. Geophys. Res., 86*, 4471-4492, 1981.

5. D.S. Orlowski, G.K. Crawford, and C.T. Russell, Upstream waves at Mercury, Venus and Earth: Comparison of properties of One Hertz waves, *Geophys. Res. Lett., 17*, 2293-2296, 1990.

6. D.S. Orlowski and C.T. Russell, ULF waves upstream of the Venus bow shock: properties of One-Hertz waves, *J. Geophys. Res., 96*,11271-11282, 1991.

7. D.S. Orlowski, C.T. Russell, D. Krauss-Varban and N. Omidi, On the source of upstream whistlers in the Venus foreshock, Plasma environments of nonmagnetic planets edited by T.I. Gombosi, p.217-227, Pergamon Press Oxford, 1993.

8. R.J. Fitzenreiter, J.D. Scudder, and A.J. Klimas, Three-dimensional analytical model for spatial variations of the foreshock electron distribution function: Systematics and comparison with ISEE observations, *J. Geophys. Res. 95*, 4155-4169,1990.

9. D.D. Sentman, M.F. Thomsen, S.P. Gary, W.C. Feldman and M.M. Hoppe, The oblique whistler instability in the Earth's foreshock, *J. Geophys. Res., 89*, 2048-2056, 1983.